Available online at www.sciencedirect.com
ScienceDirect
Physica A 377 (2007) 435–447
PHYSICA A
www.elsevier.com/locate/physa

Dissipative solitons, wave asymmetry and dynamical ratchets

Ezequiel del Rio[a,b,*], Manuel G. Velarde[b], Werner Ebeling[b,c]

[a]Dpto. Fisica Aplicada, E.T.S.I. Aeronauticos, Universidad Politecnica de Madrid, Plaza Cardenal Cisneros 3, 28040-Madrid, Spain
[b]Instituto Pluridisciplinar, Universidad Complutense de Madrid, Paseo Juan XXIII n. 1, 28040-Madrid, Spain
[c]Institut für Physik, Humboldt-Universität Berlin,Newtonstr. 15, 12489-Berlin, Germany

Received 24 May 2006
Available online 18 December 2006

Abstract

Unidirectional solitonic wave-mediated transport is shown to be possible for a class of anharmonic lattice problems where, due to wave asymmetry, the waves can be used as a traveling periodic ratchet. Using a (mesoscopic) probabilistic description we have assessed the role of both viscous friction and temperature in both the direction of transport and its quantitative features. No asymmetry is required on the potential. Furthermore its actual form and even that of the periodic wave, save its asymmetry, play no significant role in the results obtained and hence they exhibit rather universal value.

Keywords: Brownian motors; Drifting ratchet; Anharmonicity; Dissipative solitons

1. Introduction. Wave mediated transport and lattice model-dynamics

Surface waves can be broadly classified as either oscillatory or translatory. Oscillatory waves are periodic in character, imparting to the liquid an undulatory motion with both horizontal and vertical components without causing appreciable displacement. Indeed in each period a fluid particle combines its motion round a circle with forward movement through a distance (Stokes drift) varying as the square of the radius of that circle. Stokes drift represents a second-order correction to the paths of fluid particles according to linear theory [1].

Translatory waves, on the contrary, cause a net displacement of the liquid in the direction of the wave motion. Solitary waves or solitonic periodic waves, usually, "shallow" water waves are waves of translation. For nonlinear translatory waves, directed drift or transport is thus first-order effect. In the extreme case of real shallow water the liquid is set in motion over the full depth with nearly constant velocity over any cross section at any instant.[1]

*Corresponding author. Tel.: 34 91 3366302; fax: 34 91 3366303.
E-mail address: edelrio@aero.upm.es (E. del Rio).

[1]In general, however, waves in their rapid motion across the surface like tsunami in the ocean with speeds over 500 km/h traveling over water depths of 2–4 km do not move the whole water mass itself at such breakneck speeds. Water moving at high speed behaves almost as solid as concrete. If, as a usual thing, the water itself were to move with the speed of the waves ships would never have been invented. No structure we could build would be strong enough to take the pounding it would get [2].

0378-4371/$ - see front matter
doi:10.1016/j.physa.2006.11.062

Wave-mediated, directed transport has been advocated in the context of Brownian ratchets and motors [3–15]. In particular (deterministic and stochastic) Stokes drift has been studied. Here we shall focus attention to soliton-mediated drift and hence to transport associated to nonlinear translatory waves. For illustration, rather than considering the medium as a continuum we shall consider a lattice with (anharmonic) nonlinear interactions between its units. We shall restrict consideration to only longitudinal modes of motion. To be specific we shall take a Toda lattice [16] although similar results can be obtained using Morse interactions or other strongly repulsive interactions. Indeed the Morse potential is not too different from the Lennard–Jones interaction [17–25]. The choice of Toda lattice is dictated by two facts: on the one hand experimental interactions are easy to implement electronically [26] and, on the other hand, by its solutions are known analytically. It is a Hamiltonian and integrable system. It possesses solitary and periodic cnoidal waves that can travel freely along the lattice at supersonic speed. In our case here we shall take into account that realistic systems are bound to dissipate energy and hence we shall augment the conservative Hamiltonian dynamics with an appropriate input–output energy balance thus ensuring the robustness and long lasting character of the solitonic solutions. We shall be working with parameter values such that the dissipation-modified solutions depart little from the exact solutions of the conservative Toda lattice save their asymmetry around maxima. The adequacy of such choice has recently being assessed by comparing analytical results, numerical simulations and experimental results obtained with the electronic implementation of the system, i.e., with the electrical circuit equivalent to the original mechanical lattice [27,28]. The latter approach has been done following earlier work for the original conservative lattice [29,30].

The Hamiltonian of the Toda lattice is

$$H = \sum_j \left[\frac{p_j^2}{2} + \frac{\omega_0^2}{b} \mathrm{e}^{b(x_{j-1}-x_j-\sigma)} \right], \tag{1}$$

where x and p denote space and momentum coordinates, ω_0 denotes frequency (to be specified below), b is the stiffness of the mechanical springs, σ is the mean interparticle distance and Δx_j is the displacement of particle j from its equilibrium position, σ_j. As shown in Ref. [20] any exponentially decaying repulsive force with potential $v(x)$ can be locally approximated by a Toda force by using the Taylor expansion

$$v(x) = v(x_0) + (x - x_0)v'(x_0) + \frac{1}{b_0} m\omega_0^2 [\mathrm{e}^{-b(x-x_0)} - 1 + b(x - x_0)] + \text{higher-order terms}. \tag{2}$$

Thus we see that the first contribution is the harmonic oscillator, and subsequent Taylor terms correspond to the asymmetric Helmholtz potential [31], the symmetric Duffing oscillator and so on [32]. On the other hand for large values of the stiffness ($b \to \infty$) the potential approaches the impulsive hard sphere (rod) interaction. Note that the physically meaningless constant and the linear terms in Eq. (2) are not significant for our purpose here.

As earlier noted we shall augment the Hamiltonian dynamics with an appropriate energy pumping balancing the expected dissipation. Accordingly we shall consider a lattice where the Newton equations in suitable dimensionless variables for the units are

$$\begin{aligned} \frac{\mathrm{d}x_j}{\mathrm{d}t} &= p_j, \\ \frac{\mathrm{d}p_j}{\mathrm{d}t} &= \omega_0^2 (\mathrm{e}^{b(x_{j-1}-x_j-\sigma)} - \mathrm{e}^{b(x_j-x_{j+1}-\sigma)}) + (\mu - p_j^2) p_j, \end{aligned} \tag{3}$$

with $x_j = \sigma j + \Delta x_j$. At equilibrium $\Delta x_j = 0$. Further we shall consider a lattice ring, hence periodic boundary conditions (b.c.) $\Delta x_1 = \Delta x_{(N+1)}$. The system possesses the following independent parameters: ω_0 is the oscillation frequency of the harmonic approximation to (1), b has already been defined, and μ is the "pumping" parameter.

The second term in Eq. (3) demands clarification [33–35]. The currently most popular approach to maintain harmonic oscillations in the presence of dissipation is that first introduced by van der Pol [36]. It has proven useful in many realms of science and technology from physics to engineering to neurodynamics. Dissipation usually appears through a term proportional to velocity or momentum, p, added to the conservative Newton's

equation of the oscillator. Van der Pol added to the dissipative harmonic oscillator equations a term proportional to the square of the elongation of the motions, x^2. By doing this van der Pol transformed the harmonic oscillator into a nonlinear oscillator exhibiting limit cycle oscillations, hence maintained, robust vibrations.

The choice made by van der Pol is not the only possible choice. Indeed, much before van der Pol, Lord Rayleigh [37,38] suggested adding a term proportional to the square of the velocity, v^2, or the momentum, p^2. Thus, he introduced a friction force like $\gamma v\ (1 - v^2)$ with γ the corresponding friction coefficient. After suitable redefinition of the latter coefficient and using and appropriate reference velocity scale [34,35] the friction force can be expressed in the form shown in Eq. (3) $(\mu - p^2)p$, using p rather than v. Hence this friction force contains both dissipation (*passive* friction) μp (positive on the right-hand side of (3)) and a term $(-p^2 p)$ that has been called *active* friction. With Lord Rayleigh's choice we ensure that by varying the value of μ the oscillations can be maintained. Clearly there is a value of μ such that system (3) becomes conservative, and indeed we recover the Toda model. Other forms of *active* friction are available in the literature [34,35]. One way to visualize Lord Rayleigh's idea is to think about the feedback upon a violin string of the multimodal energy accumulated in the instrument's bow. This multimodal energy appears as a kind of noise bath for the string. As we plan to consider Brownian particles immersed in a heat bath we shall retain Lord Rayleigh's energy pumping function.

We have extensively studied Eq. (3) [21,22,25,27,28]. At $\mu = 0$ there is bifurcation from the motionless case to wave propagation along the lattice. In Section 2 we recall solutions of Eq. (3) with a significant feature, the asymmetry around the peak of a solitary wave or around all peaks for quasi-cnoidal periodic waves. It has been shown in Ref. [20] that an external harmonic driving wave, likely to be performed by a suitable piezoelectric excitation, creates about the same solitonic waves. Here we only need the (asymmetric) wave form, not the actual means of excitation. Section 3 is devoted to the description of the drifting solitonic ratchet using a suitable sawtooth approximation. The motion of *active* Brownian particles in a *static* sawtooth has been studied in Ref. [39]. In Section 4 we discuss the role of noise level and hence temperature upon transport. Finally, in Section 5 we provide a summary of results and a few concluding remarks.

2. Lattice ring, wave propagation and wave asymmetry

Let us consider a 1D lattice composed of units as shown in Fig. 1. As earlier noted we shall restrict attention to the case with periodic b.c. hence to a lattice ring. It has been shown analytically, numerically and experimentally using the electric analog circuit or computer (Fig. 2) [27,28] that along such lattice ring periodic quasi-cnoidal waves and solitary waves can stably travel. Fig. 3 depicts one such wave for $N = 6$. This is not the only wave possible. Indeed, with N units in the ring there are $(N - 1)$ wave modes possible. For N even there is also an optical-like mode with units longitudinally vibrating in antiphase. Noticeable in Fig. 3 is the asymmetry of the wave peaks, a feature shared by all other modes in the system save the "optical"-mode. The highest asymmetry occurs for the mode $m = 1$ (or its symmetric $m = -1$. The latter possess "negative" velocity which denotes motion in the opposite direction to that of the former; the $m = -1$ is also obtained by the appropriate $t \to -t$ time inversion). The quasi-cnoidal wave travels with velocity $v = \sigma\lambda/\tau_0 = (\sigma\lambda/2\pi)\omega_1$,

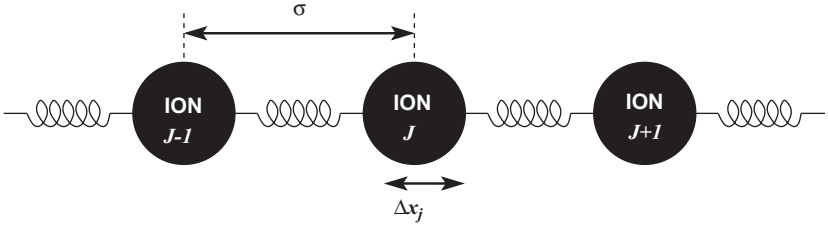

Fig. 1. Toda lattice. Three units (ions) interacting through *anharmonic* "springs". σ is the mean distance between units, Δx_j is the displacement from the equilibrium position of unit "j".

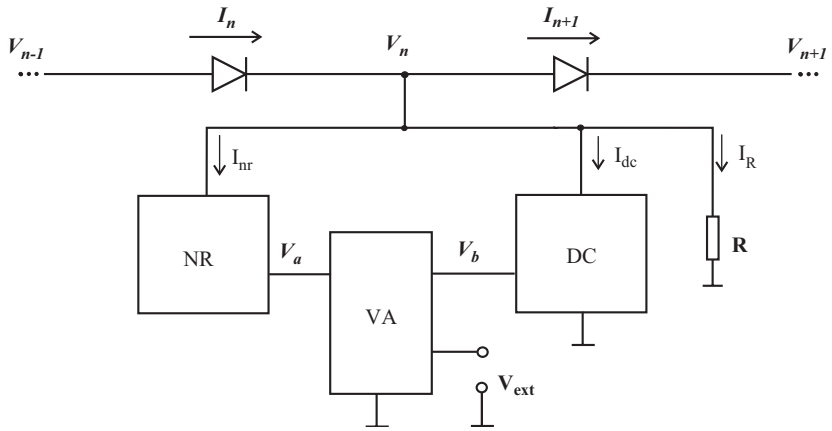

Fig. 2. Analog electronic unit, building block or element ($1 \leqslant n \leqslant N$) of the corresponding lattice ring (Fig. 1) with Newton equations (3). V and I denote voltage and current intensity, respectively. DC is a double capacitor [26], NR a nonlinear resistor, VA is a voltage adder with inputs V_a and V_{ext} and output V_a.

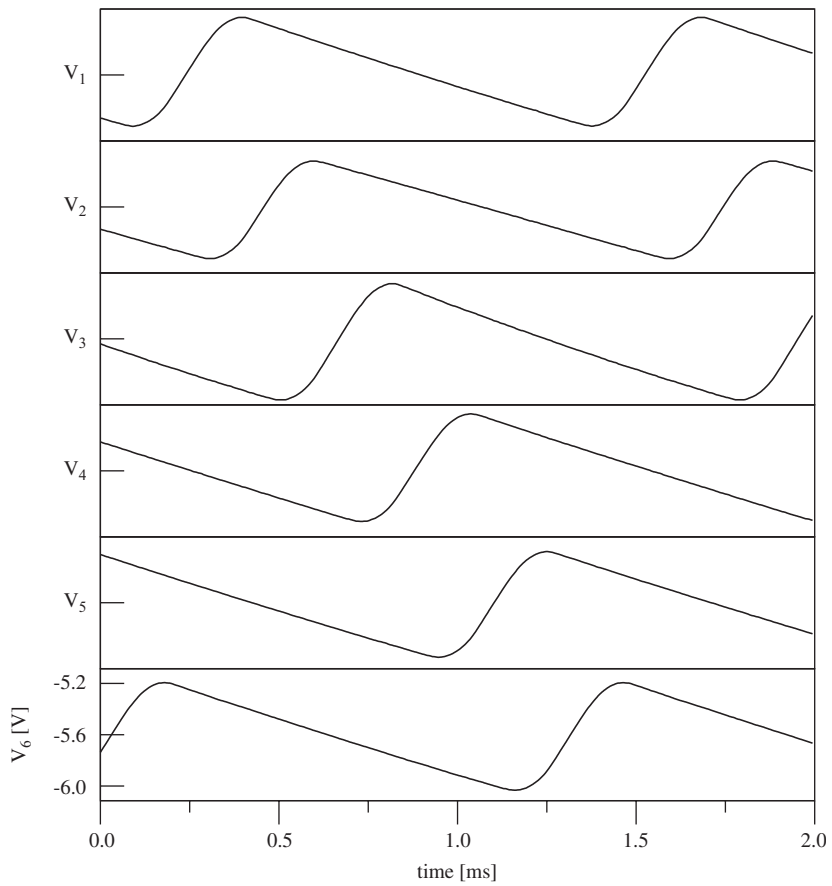

Fig. 3. Waveform in the analog circuit of a lattice ring with $N = 6$ units as in Fig. 6. The wavetravels down while the "longitudinal" motions of the units bring them all left to right. Experimental data correspond to voltage *versus* time at a given point (as it appears in the oscilloscope).

where τ_0 denotes its period and ω_1 is the angular frequency ($m = 1$),

$$\omega_m = 2\omega_0 \sin\frac{\pi m}{N}\left(1 + \frac{\mu}{12\omega_0^2}\right), \tag{4}$$

which defines m.

3. Traveling solitonic ratchet

Let us now consider the units in the original mechanical lattice ring as *heavy ions* and let us add a *light* particle in 3D-geometry to rule out unnecessary singularities due to (1D and 2D) geometry. The light particle can be an "electron", and hence with opposite albeit equal charge to the ions, the electron–lattice interaction can be taken, e.g., as

$$U_e(r) = \frac{-U_0}{\sqrt{1 + r^2/h^2}}, \tag{5}$$

or

$$U_e(r) = -U_0 \mathrm{e}^{-r^2/2h^2}, \tag{6}$$

which is a Gaussian well. In both cases, U_0 is the maximum and h is the minimal distance allowed between the light electron and the heavy ions, $h < \sigma$. We shall see that the particular choice of such interaction plays no significant role.

As earlier emphasized, in the case we are interested here (Eq. (3)) and that we have dealt with recently [27,28] solitonic waves or excitations are described, e.g., by combinations of elliptic functions like cnoidal and quasi-cnoidal waves [16]. Then in view of Fig. 3 we can approximate the actual waveform by a *sawtooth* function, such that

$$\Delta x_j = A\psi\left(\frac{j}{\lambda} - \frac{t}{\tau_0}\right), \tag{7}$$

where

$$\psi(z+1) = \psi(z) = \begin{cases} \lambda z & \text{if } z \in S_1 = \left[0, \dfrac{1}{\lambda}\right), \\ \dfrac{\lambda}{\lambda - 1}(1 - z) & \text{if } z \in S_2 = \left[\dfrac{1}{\lambda}, 1\right]. \end{cases} \tag{8}$$

The quantities A, τ_0 and λ correspond to amplitude, period and wave-length (number of units), respectively. Fig. 4 illustrates the choice done for $m = -1$ for $\lambda = 6$ and $A = 1.2$, with $v = -\sigma\lambda/\tau_0$.

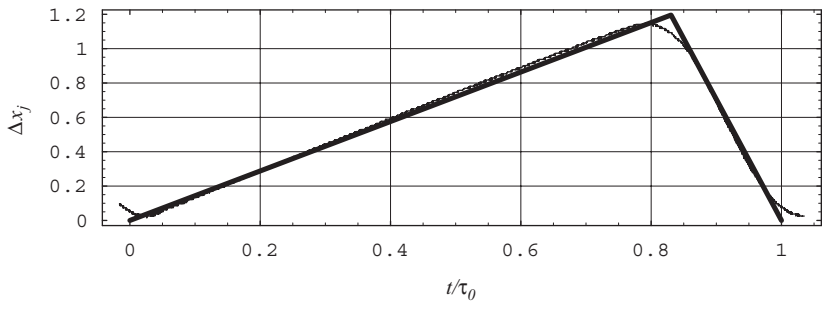

Fig. 4. Dissipative Toda lattice. Sawtooth approximation to the waveform depicted in Fig. 3 (for convenience we have taken the equivalent symmetric form). Parameter values: $\lambda = 6$ and $A = 1.2$. For convenience we have taken the equivalent left moving waveform.

Using the sawtooth approximation the overall electron–lattice interaction potential for the light particle placed at position y can be explicitly expressed in the following form:

$$U(t,y)=\sum_{j=n_y-n}^{n_y+n}U_e(x_k-y)=\sum_{j=n_y-n}^{n_y+n}U_e\left(\sigma j+A\psi\left(\frac{(\sigma/v_w)j-t}{\tau_0}\right)-y\right). \tag{9}$$

Taking $y=n_y\sigma+\Delta y$, with $|\Delta y|<\sigma$, we can safely neglect in Eq. (9) the contributions arising from lattice units beyond $n\sigma$. Noteworthy is that in the present case the wave group velocity is time-dependent at variance with the standard traveling ratchets [40,41] and the Brownian surfer considered in Ref. [42].

However "light" the electron is relative to the "heavy" lattice ions, we shall take it Brownian in a thermal bath surrounding the entire system. Accordingly, it obeys the following Newton's (Langevin) equation of motion:

$$\frac{\mathrm{d}^2y}{\mathrm{d}t^2}+\gamma\frac{\mathrm{d}y}{\mathrm{d}t}+\frac{\partial U(t,y)}{\partial y}=\gamma\sqrt{2D}\xi(t), \tag{10}$$

with γ and D, both positive, account for viscous friction and spatial diffusion, respectively. The noise is taken white Gaussian of zero mean and delta-correlated in time. Further ξ, γ and D obey the fluctuation–dissipation theorem and Einstein's relation, thus the noise strength or level, k_BT, provides the temperature, T, of the bath; k_B denotes Boltzmann's constant [43,44].

Let us analyze the behavior of the potential (9) due to wave propagation with the sawtooth peaks. Its extrema are obtained by setting

$$\frac{\partial U(t,y)}{\partial y}=-\sum_{j=n_y-n}^{n_y+n}U_e'\left(\sigma j+A\psi\left(\frac{(\sigma/v_w)j-t}{\tau_0}\right)-y\right)=0. \tag{11}$$

On the other hand the time-derivative of Eq. (11) permits to obtain the local speed of points with $\partial U(t,y)/\partial y=constant$, and, needless to say of the extrema. Thus we have

$$\frac{\mathrm{d}y}{\mathrm{d}t}=\frac{A}{\tau_0}\frac{\lambda}{\lambda-1}\frac{\sum_{j\in j_2}U_{ej}''-(\lambda-1)\sum_{j\in j_1}U_{ej}''}{\sum_{j\in j_2}U_{ej}''+\sum_{j\in j_1}U_{ej}''}, \tag{12}$$

with

$$U_{ej}\equiv U_e\left(\sigma j+A\psi\left(\frac{(\sigma/v_w)j-t}{\tau_0}\right)-y\right), \tag{13}$$

where the subscript j_1 indicates S_1 in Eq. (8), i.e., ψ is evaluated at point P_1 in Fig. 5a, along the side of positive slope. Accordingly, j_2 refers to a point like P_2 in Fig. 5a in the region of negative slope. It appears that $\mathrm{d}y/\mathrm{d}t$ does not depend on U_0, and that Eq. (12) reflects the discrete lattice character of the system.

Two significant cases exist. One appears when

$$\left|\sum_{j\in j_2}U_{ej}''\right|\gg(\lambda-1)\left|\sum_{j\in j_1}U_{ej}''\right|, \tag{14}$$

and the other corresponds to the opposite situation

$$\left|\sum_{j\in j_2}U_{ej}''\right|\ll(\lambda-1)\left|\sum_{j\in j_1}U_{ej}''\right|. \tag{15}$$

In the former case (14) it can be seen that the contribution of points along the side of the sawtooth with positive slope to the speed of the light particle is not significant, hence it can be neglected. Thus according to Eq. (12) we can write $\mathrm{d}y/\mathrm{d}t\approx v_1=\lambda/(\lambda-1)A/\tau_0>0$, which is the speed of the lattice units in the P_1 region of Fig. 5a. In the other case, the velocity is $\mathrm{d}y/\mathrm{d}t\approx v_2=-\lambda A/\tau_0<0$, the value corresponding to the lattice particles in region P_2 of Fig. 5a. As a matter of fact, if h is so short that once the light particle is bound to a given lattice unit so that we can neglect the influence of the other lattice particles, then condition (14) or (15) is

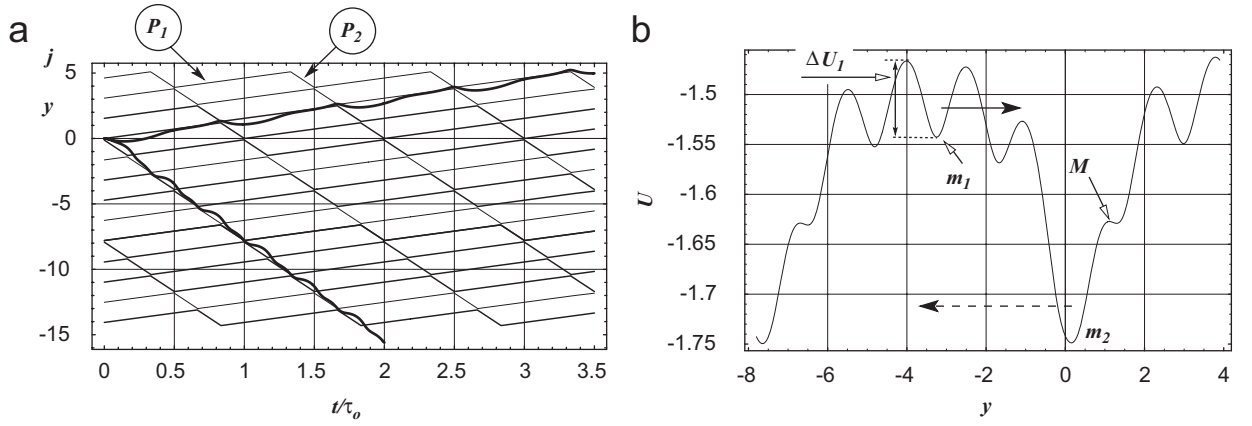

Fig. 5. (a) Trajectories of 13 heavy ions and two non-interacting (hence free) *light* particles for $\gamma = 2.51$ (motion left to right) and $\gamma = 0.29$ (opposite direction of motion or negative velocity). (b) The snapshot of the potential is captured for $U_0 = 0.47$ and $h = 0.43\sigma$.

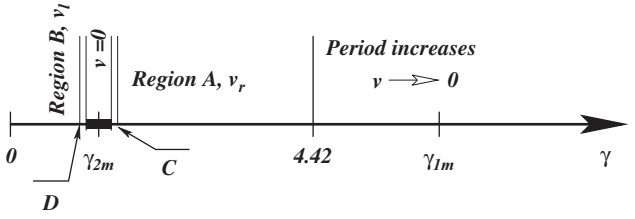

Fig. 6. Different attractor regions offered to the *light* particle according to the values of γ, with $\gamma_{1m} = 5.29$ and $\gamma_{2m} = 1$.

satisfied, provided the particles are in region P_1 or P_2, respectively. If, however, h is much large relative to σ, neither (14) nor (15) is satisfied and the potential will follow the direction of wave motion and no minima, m_1, appears in the corresponding Fig. 5b. The computations have been done using

$$U_e(y - x_k) = -U_0/[1 + (y - x_k)^2/h^2]^{1/2}, \tag{16}$$

under the assumption that (free) "electrons" cannot penetrate (screened) ion cores. The pseudopotential (16) is of current use in the literature [45].

If at given instance, condition (14) is satisfied, we expect periodically spaced regions where the (potential) wave moves left to right as point m_1 in Fig. 5b. Alternatively, when condition (15) is satisfied the (potential) wave will accordingly proceed right to left, as points m_2 in Fig. 5b. Note the key role played by the value of h in Eq. (16). Yet the actual wave form plays little role save its asymmetry. As $\lambda \neq 2$ the ratchet is asymmetric with $|v_1| \neq |v_2|$.

In the noiseless case, there are values of γ for which the light particle moves with positive velocity (left to right; region A in Fig. 6) $v_r = \lambda/(\lambda - 1)\sigma/\tau_0 > 0$, slightly different from v_1. This is due to the fact that the light particle periodically jumps when it finds a minimum traveling in opposite direction. Besides, there are regions of values of γ where the light particle moves with negative speed (region B in Fig. 5), $v_l = v_w < 0$. In this latter case the light particle speed is higher (in absolute value) than the velocity of the lattice particles. Both above given cases are depicted in Fig. 5.

Let us now study the behavior of the light particle in the neighborhood of the minima as a function of the values of the parameter γ accounting for viscous friction. We take a washboard potential by means of a suitable Galilean transformation [42], $y = z + v_1 t$, and then Eq. (10) becomes

$$\frac{d^2 z}{dt^2} + \gamma \frac{dz}{dt} + \frac{\partial(U + \gamma v_1 z)}{\partial z} = \gamma\sqrt{2D}\xi(t). \tag{17}$$

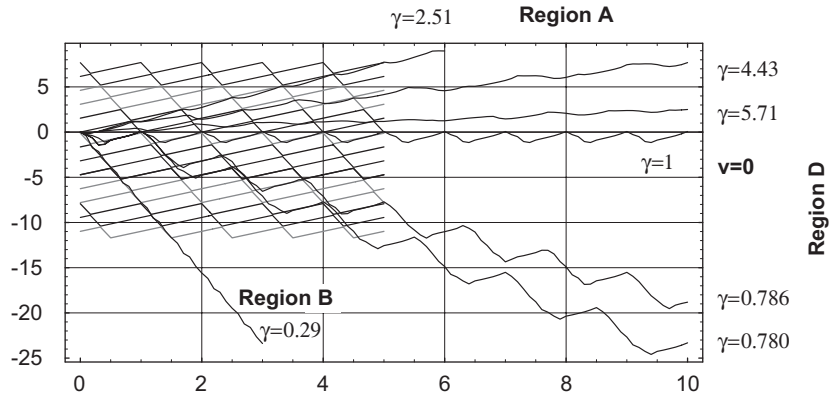

Fig. 7. Light particle trajectories corresponding to five values of γ in accordance with the regions depicted Fig. 6. For $t/\tau_0 < 5$ the trajectories of a few lattice particles are also displayed. Abcissa: t/τ_0.

Our case bears similarity with the Brownian *surfer* analyzed in Ref. [42], save that ours has a local velocity (note that a surfer rides the traveling wave while a swimmer dynamically travels on the surface of the ocean).

It appears that the potential in Eq. (17) possesses a stationary minimum, corresponding to the well of m_1 in Fig. 5b, if γ is below $\gamma_{1m} \approx U'_{max}/v_1$ where U'_{max} is the maximum of U' in between the maximum of U previous to the minimum m_1 and m_1. So for $\gamma > \gamma_{1m}$ there are time intervals where $(U + \gamma v_1 z)$ exhibits no minima. Then the potential in Eq. (10) does not provide enough energy to the light particle to allow it maintaining its speed v_1 (see Fig. 5a). Such is the case for $\gamma = 5.71$ shown in Fig. 7. The light particle remains oscillating in the potential well offered by a lattice particle, until the possibility appears to jump to the next available potential well of the nearest nearby lattice particle. Thus we shall see long lasting trajectories (long time periods) and low speeds as the value of γ increases as shown in Fig. 6. Actually, the upper bound of region A covers values below γ_{1m} as $v_r > v_1$ ($\gamma = 4.42$ in Fig. 6). This argument applies *verbatim* to the minimum m_2 in Fig. 5b provided use is made of the Galilean transformation $y = z + v_2 t$ leading to the potential value $(U + \gamma v_2 z)$. In this case we have a value γ_{2m} such that for $\gamma > \gamma_{2m}$the light particles cannot pump enough energy to be able to maintain the speed v_2. Here $\gamma_{2m} < \gamma_{1m}$, and the light particles in region A of Fig. 6 have speed v_r ($\gamma = 2.51$ in Fig. 7, trajectory with positive velocity in Fig. 5a). In region B of Fig. 6 the potential barrier $(U + \gamma v_2 z)$ is higher than the other one $(U + \gamma v_1 z)$ and the light particle takes on negative speed ($\gamma = 0.29$, Fig. 5a). Such behavior in regions A and B bear similarity with the description given in Ref. [40] in the *noiseless* case. There is also similarity with the *noiseless* and the *traveling* solutions described in Ref. [44] which in our case would appear as jumps over the potential barrier ΔU_1 in Fig. 5.

Between regions A and B an alternative appears: motion with positive speed in one minimum or in another with negative speed. Near $\gamma = \gamma_{2m}$ (thicker black region in Fig. 6) the speed is zero as the particle moves back and forth around the same lattice unit ($\gamma = 1$ trajectory in Fig. 7). Between this region and regions A and B *numerous* possibilities exist in the two narrow zones C and D of γ values (Fig. 6). Several possible trajectories in region D are depicted in Fig. 7. To avoid a messy graph no trajectories belonging to region C have been drawn. Indeed, for $\gamma = 4.43$ and 5.71 they practically overlap each other.

To be noted is that we have no γ-related hysteresis here at zero temperature, at variance with cases discussed in the literature [42]. Yet, as earlier indicated, we do not have a single phase wave velocity.

In view of the above, we can conclude that for values of γ in the regions A and B the quasi-cnoidal periodic waves operate along the lattice as typical ratchets (traveling or drifting ratchets).

4. The role of noise and temperature upon transport

Let us now discuss the role of noise in the system for values around γ_{2m} and in region A. One may expect that the noise strength alters the direction of motion. For low noise level, particles with γ in the region A, move within a potential minimum (Fig. 5b, m_1) with velocity $v_r > 0$, in opposite direction to the solitonic wave. After

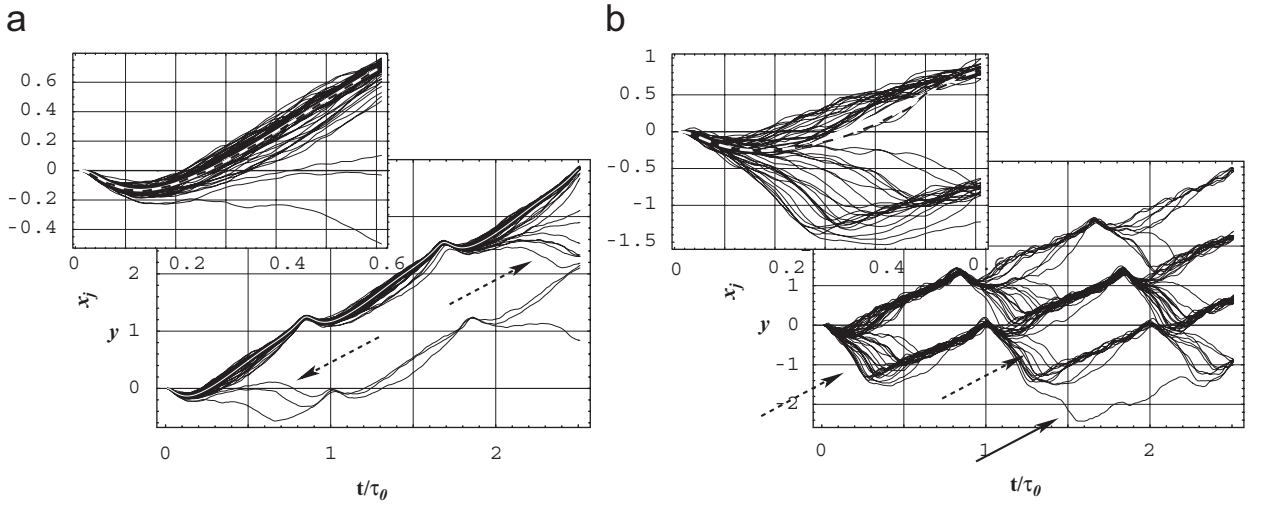

Fig. 8. Light particle trajectories. 50 realizations starting from the same initial condition ($y = \mathrm{d}y/\mathrm{d}t = 0$) zoomed for $t/\tau_0 < 0.6$. The dashed white line is the *deterministic* trajectory. Parameter values: (a) $\gamma = 2.54$; and (b) $\gamma = 1.43$. See points a and b in Fig. 10.

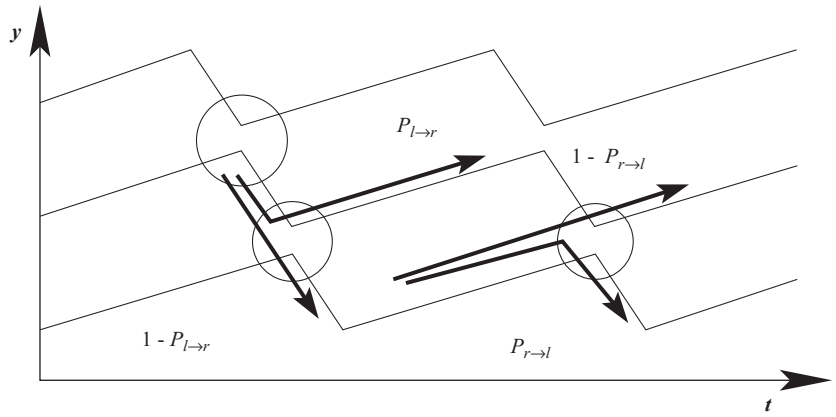

Fig. 9. Dissipative Toda lattice. Three units are used to display four light particle trajectories with their corresponding probabilities.

some time lapse, they take on a deeper nearby available minimum (Fig. 5b, m_2) and travel with negative speed higher in absolute value and hence in the soliton motion direction. Then due to the noise level, the particle may change its direction of motion, transferring to another minimum, with *conditional* probability, $P_{r\to l}$, Fig. 8. If such is the case (trajectories noted with broken arrows in Fig. 8), a fraction of period later it finds another minimum traveling with $v_r > 0$ and hence the particle has probability $P_{l\to r}$ to return to its previous antisolitonic motion. In Fig. 8a, $P_{r\to l} < 1$ although $P_{l\to r} \approx 1$. This is due to the fact that all trajectories with negative speed (indicated by the broken arrows) change to positive velocity as soon as they see nearby a minimum with one such velocity. This is not the case for Fig. 8b, where trajectories with negative velocity keep their velocity even after meeting a minimum with positive velocity (noted with an arrow in Fig. 8b). Thus two different underlying mechanisms control $P_{r\to l}$ and $P_{l\to r}$.

For a Brownian particle we can estimate its mean velocity, v_B, in term of these two probabilities. It suffices to consider the evolution of a particle over a long enough time interval, T_0. Fig. 9 depicts several lattice compressions, nodes (three are marked with open circles) along with four paths (see Fig. 8, and corresponding conditional probabilities).

Let N_l denote the total number of steps towards the left (up–down in Figs. 8 and 9) done by a particle in the time lapse T_0. The quantity N_r refers to the opposite case (down–up motions in Figs. 8 and 9). Let the time duration of each step be t_l and t_r, respectively. The total time lapse is $T_0 = (t_l N_l + t_r N_r)$ for $N = N_l + N_r$ steps. The mean velocity is

$$v_B = \frac{\sigma(N_r - N_l)}{t_r N_r + t_l N_l}. \tag{18}$$

As Fig. 9 shows, the particle may change direction of motion at each node. Let $N_{l\to r}$ be the total number of steps from left to right, and $N_{r\to l}$ in the opposite case. If the number of steps is high enough, we can write $P_{l\to r}N_l = N_{l\to r}$ and $P_{r\to l}N_r = N_{r\to l}$. As $N_{l\to r} = N_{r\to l}$, we have

$$\frac{N_l}{N_r} = \frac{P_{r\to l}}{P_{l\to r}}. \tag{19}$$

Then from (18) and (19) follows

$$v_B = \frac{1 - P_{r\to l}/P_{l\to r}}{1 - (V_r/V_l)P_{r\to l}/P_{l\to r}} v_r = \frac{1 - (P_{r\to l}/P_{l\to r})}{\lambda - 1 + (P_{r\to l}/P_{l\to r})} \frac{\lambda\sigma}{\tau_0}, \tag{20}$$

where use has been made of $t_r = \sigma/v_r$ and $t_l = \sigma/v_l$. Note that if (8) is *symmetric*, $\lambda = 2$, as $P_{r\to l} = P_{l\to r}$, it follows $v_B = 0$, whatever the noise level and hence the value of the temperature. On the other hand, if $v_B = 0$ at zero temperature, around γ_{2m} and $\lambda \neq 2$ when (8) is asymmetric, then for nonvanishing temperature, $P_{r\to l} \neq P_{l\to r}$, and hence v_B may be positive or negative as we shall discuss further below (see $\gamma = 1.14$ in Fig. 10).

Let us estimate the probabilities $P_{r\to l}$ and $P_{l\to r}$ and hence the velocity v_B. According to Fig. 8 the upward moving Brownian particle trajectories remain within a tube of positive velocity around the deterministic trajectory (broken line, Fig. 8). Those particles far away than x_0 change direction of motion even in the absence of noise at a node as the nearest lattice unit does so. In Fig. 8a around nodes we see that not all trajectories below the deterministic path change direction. However, in Fig. 8b, all trajectories below the deterministic one do change direction of motion, hence $x_0 \approx 0$. The value of x_0 depends on γ in region A. The nearer is the value of the latter parameter to the lower boundary of such region, the lower is the distance x_0 acceptable for the trajectory to remain around the deterministic path, x_{det}.

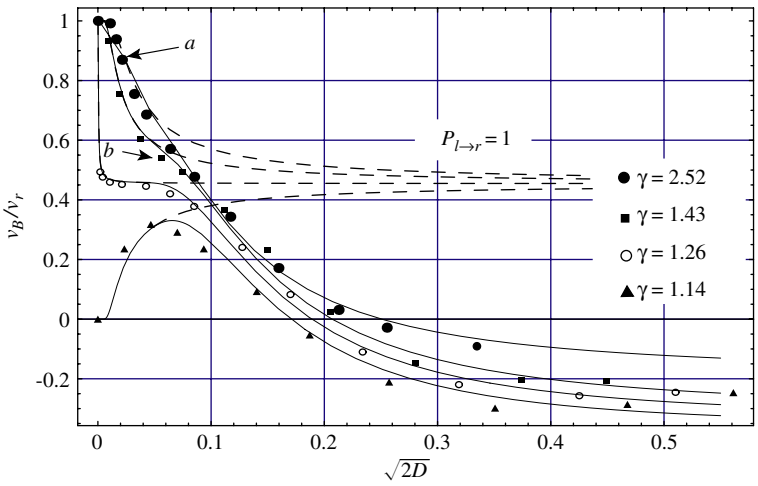

Fig. 10. Normalized mean velocity (v_B/v_r) of one hundred Brownian particles *versus* noise level $\sqrt{2D}$. Curves are parameterized by γ. Results obtained by direct numerical integration of Eq. (10) during a time lapse of $2000\tau_0$. Solid lines correspond to the approximation equation (20) with (22) and (24) for the three upper curves. For $\gamma = 1.14$, lower curve, Eq. (22) is to be substituted by Eq. (26). The dashed lines correspond to Eq. (20), with $P_{l\to r} = 1$. Parameter values common to all curves: $t_0 = 0.2\tau_0$, $t_1 = 0.05\tau_0$, $\omega = 4.2$, $\Delta U = 0.01$. For x_0, which depends on γ, we have $\gamma = 2.52 \to x_0 = 0.07$, $\gamma = 1.43 \to x_0 = 0.045$, $\gamma = 1.26 \to x_0 = 0.001$ and $\gamma = 1.14 \to x_0 = 0.05$.

The behavior of the particles in the tube can be approximately described by a *diffusive* stochastic process around x_{det}, with

$$P(x_{det}|x;t_0)=\frac{1}{2\sqrt{\pi D t_0}}\mathrm{e}^{-\frac{(x_{det}-x)^2}{4Dt_0}}, \tag{21}$$

where t_0 is the diffusion time needed to attain a stationary process. Accordingly,

$$P_{r\to l}=\int_{-\infty}^{-x_0}P(x_{det}|x;t_0)\mathrm{d}x=\frac{1}{2}\mathrm{erfc}\left(\frac{x_0}{2\sqrt{Dt_0}}\right). \tag{22}$$

Clearly (22) is like the probability associated to the diffusion over a hard obstacle in absolute negative mobility (ANM) processes for relatively long times [3]. In our case the hard wall comes from the potential barriers ΔU_1 (Fig. 6). The end of the wall is the position, albeit time-dependent of the maximum M. Note that the time lapse t_0 is significant only when the values of γ are far enough from the minimum in region A. Otherwise, $x_0\approx 0$ and very quickly $P_{r\to l}\to\frac{1}{2}$.

On the other hand, $P_{l\to r}$ is related to the escape probability, P_{esc}, from a local potential minimum, hence $P_{l\to r}=1-P_{esc}$. At variance with the ANM case here, a priori, we cannot neglect this probability as the minimum moves up as time proceeds. In standard ratchet studies [4,5] the variations of the potential are generally taken adiabatic hence neglecting the transition times relative to the time lapse where the sawtooth operates. This together with the rather high level of the potential barrier makes negligible the probability of the Brownian particle to jump over. In our case the growth of the barrier from zero to its maximum is due to the oscillatory motion of the lattice units with period about τ_0/λ. Then the Brownian particle has such a time internal to escape with probability P_{esc}. This probability can be estimated using Kramers' formula [43,44]

$$P_{esc}=\int_0^{t_1}\alpha\mathrm{e}^{-\alpha t}\mathrm{d}t\quad\text{and}\quad\alpha=\Gamma\mathrm{e}^{-\Delta U\gamma/D}, \tag{23}$$

where ΔU is an adjustable parameter as the potential barrier does not remain constant. As ΔU does not depend on γ in the time lapse under consideration, we can write

$$P_{l\to r}=\mathrm{e}^{-\alpha t_1}. \tag{24}$$

In our case, the value t_1 in (23) or (24) is approximately $t_1\approx 0.12\tau_0$. The escape rate α contains the usual Arrhenius factor and the preexponential factor Γ. In the intermediate to high dissipation (IHD) limit [6,43]

$$\Gamma=\frac{\omega_a}{2\pi}\left(\sqrt{1+\frac{\gamma^2}{4\omega_c^2}}-\frac{\gamma}{2\omega_c}\right), \tag{25}$$

where ω_a and ω_c denote the frequencies corresponding to the potential minimum and maximum, respectively. In our case they are approximately equal, $\omega_a=\omega_c=\omega$. Note that the IHD approximation refers to stationary processes. In our case the stationary probability is attained in a time lapse much shorter than any ratchet characteristic time.

Introducing (22), (24) in (20) we get the velocity as shown in Fig. 10, where we plot v_B/v_r versus γ. It appears that for relatively high values of γ ($\gamma=2.51$) the distance x_0 is large enough for the system not to be so much sensitive to diffusion (responsible of the growth of $P_{r\to l}$ from zero to about 0.5). This is not so for $\gamma=1.26$ when the system is near the boundary of region A. There x_0 is so small and it suffices a slight backward motion of the Brownian path relative to the deterministic trajectory to loose a step forward. Then v_B is very sensitive to temperature near zero. Lowering γ to $\gamma=1.14$ we enter the region with $v=0$ (Fig. 6; see also the trajectory in Fig. 7). Then all particles reflected backward relative to the deterministic trajectory do not affect the mean velocity value. On the contrary, those particles scattered forward gain one step further thus yielding a positive mean velocity. Accordingly, in the *noiseless* case $P_{r\to l}=1$ whereas $P_{r\to l}\to\frac{1}{2}$ as the noise level increases. In view of the above, Eq. (22) becomes

$$P_{r\to l}=1-\int_{x_0}^{-\infty}P(x_{det}|x;t_0)\,\mathrm{d}x=\frac{1}{2}\left(1+\mathrm{erf}\left(\frac{x_0}{2\sqrt{Dt_0}}\right)\right), \tag{26}$$

and so in Eq. (20) we must use (26) rather than (22) as earlier done. In Fig. 10 this case is depicted for $\gamma = 1.14$ together with the result of the direct numerical integration of Eq. (3). It appears that for nearly vanishing temperature the diffusion with $P_{r\to l}$ produces a positive mean velocity. As temperature rises, the latter effect is compensated by the evolution of $P_{l\to r}$, as in previous cases with Eq. (24). This brings once more zero velocity and change of direction of motion. Fig. 10 also depicts Eq. (20) with $P_{l\to r} = 1$, when only diffusion affects $P_{r\to l}$. The approximation appears acceptable for low temperatures only (point a in black corresponds to the parameter values of Fig. 8a). Our computations show that in such a case the escape probability over the potential barrier, $P_{l\to r}$, is practically vanishing. Indeed, we have computed N_l and N_r, Eq. (18), together with $N_{l\to r}$ and hence $P_{l\to r} \approx (N_{l\to r}/N_l)$ and $P_{r\to l} \approx (N_{l\to r}/N_r)$. For $\sqrt{2D} > 0.15$, the escape becomes significant, and the computations diverge when $P_{l\to r} = 1$. This is so because $P_{l\to r}$ decreases due to the jump over the local potential barrier and matches the analytical estimate. For instance, we can see in Fig. 10 that at point b (black) there is a tendency to depart from the dashed line. There are trajectories that upon reaching negative velocity keep it for a few steps (arrow in Fig. 8b). For high noise levels, $P_{r\to l} \to \frac{1}{2}$ and $P_{l\to r} \to \mathrm{e}^{-\Gamma t_1/2\pi}$, and hence

$$\frac{v_B}{v_r} \to \frac{2\mathrm{e}^{-\Gamma t_1} - 1}{2v_l\mathrm{e}^{-\Gamma t_1} - v_r} = \frac{2\mathrm{e}^{-\Gamma t_1} - 1}{2(\lambda - 1)\mathrm{e}^{-\Gamma t_1} + 1}\frac{\sigma\lambda}{\tau_0}. \tag{27}$$

The asymptotic value (27) is never reached. At very high temperatures the light particle takes enough energy to jump over several successive potential maxima, a case not considered in the present study. Yet such asymptotic value (27) indicates a temperature-driven change of direction in the motion of the light particle, provided

$$\Gamma t_1 > \ln 2. \tag{28}$$

5. Concluding remarks

Wave-mediated transport is first-order in nonlinear propagating waves. To implement it we have used this fact together with the ratchet character of dissipative solitons traveling along a lattice with anharmonic (exponentially repulsive) interactions. The specific form of the potential is not significant from the physical standpoint and the main results found. What matters is that such (periodic) solitons have asymmetric wave forms while the underlying potential is, generally, symmetric. As in principle those dissipative solitons may move clockwise or counterclockwise, (Brownian) light particles traveling with them (a kind of surfing) are also allowed to move in either direction. However, viscous friction helps breaking the symmetry and hence the ratchet wave mechanically separates the light particles leading to net unidirectional transport. We have determined the mean velocity and how those particles may reverse motion. We have also studied related features depending on noise strength and hence temperature. In conclusion, we have shown how the interplay of the soliton ratchet and unbiased random fluctuations does generate net transport. In view of the possible mechanical or electrical implementation of the ratchet device here described we can say that the latter can provide a method to convert mechanical or even chemical energy into net transport and, eventually, electricity.

Acknowledgments

This research has been sponsored by the European Union under Grant SPARK (FP6-004690) and by the Spanish Ministerio de Educación y Ciencia under Grant ESP2004-01511.

References

[1] J. Lighthill, Waves in Fluids, Cambridge University Press, Cambridge, 1978, pp. 279–280.
[2] B. Kinsman, Wind Waves, Dover, Mineola, New York, 1984 (Sections 10.3, 10.4).
[3] R. Eichhorn, P. Reimann, P. Hänggi, Phys. Rev. Lett. 88 (2002) 190601-4.
[4] A. Ajdari, J. Prost, C. R. Acad. Sci. Paris 315 (1992) 1635–1639.
[5] R.D. Astumian, M. Bier, Phys. Rev. Lett. 72 (1994) 1766–1769.
[6] W.T. Coffey, D.A. Garanin, D.J. McCarthy, Adv. Chem. Phys. 117 (2001) 483–490.
[7] M. von Smoluchoswski, Phys. Z. III (1912) 1069–1075.
[8] J.F. Chauwin, A. Ajdari, J. Prost, Europhys. Lett. 32 (1995) 373–378.

[9] M.O. Magnasco, Phys. Rev. Lett. 71 (1993) 1477–1481.
[10] J. Rousselet, L. Salome, A. Ajdari, J. Prost, Nature 370 (1994) 446–448.
[11] G.W. Slater, H.L. Guo, G.I. Nixon, Phys. Rev. Lett. 78 (1997) 1170–1173.
[12] P. Reimann, M. Grifoni, P. Hänggi, Phys. Rev. Lett. 79 (1997) 10–13.
[13] P. Reimann, Phys. Rep. 361 (2002) 57–365.
[14] K.M. Jansons, G.D. Lythe, Phys. Rev. Lett. 81 (1998) 3136–3139.
[15] I. Bena, M. Copelli, C. Van den Broeck, J. Stat. Phys. 101 (2000) 415–424.
[16] M. Toda, Theory of Nonlinear Lattices, Springer, Berlin, 1981.
[17] Ph. Choquard, The Anharmonic Crystal, Benjamin, New York, 1967.
[18] A.P. Chetverikov, W. Ebeling, M.G. Velarde, Eur. Phys. J. B 44 (2005) 509–519.
[19] A.P. Chetverikov, W. Ebeling, M.G. Velarde, Contrib. Plasma Phys. 45 (2005) 275–283.
[20] A.P. Chetverikov, W. Ebeling, M.G. Velarde, Eur. Phys. J. B 51 (2006) 87–99.
[21] V.A. Makarov, M.G. Velarde, A.P. Chetverikov, W. Ebeling, Phys. Rev. E 73 (2006) 066626-1-12.
[22] M.G. Velarde, W. Ebeling, A.P. Chetverikov, Int. J. Bifurc. Chaos 15 (2005) 245–251.
[23] M.G. Velarde, W. Ebeling, D. Hennig, C. Neissner, Int. J. Bifurc. Chaos 16 (2006) 1035–1039.
[24] D. Hennig, Ch. Neissner, M.G. Velarde, W. Ebeling, Phys. Rev. B 73 (2006) 024306-1-10.
[25] A.P. Chetverikov, W. Ebeling, M.G. Velarde, Int. J. Bifurc. Chaos 16 (2006) 1613–1632.
[26] P. Horowitz, W. Hill, The Art of Electronics, second ed., Cambridge University Press, New York, 1989.
[27] V.A. Makarov, E. del Rio, W. Ebeling, M.G. Velarde, Phys. Rev. E 64 (2001) 036601-1-14.
[28] E. del Rio, V.A. Makarov, W. Ebeling, M.G. Velarde, Phys. Rev. E 67 (2003) 056208-1-9.
[29] R. Hirota, K. Suzuki, Proc. IEEE 61 (1973) 1483.
[30] A.C. Singer, A.V. Oppenheim, Int. J. Bifurc. Chaos 9 (1999) 571.
[31] E. del Rio, A. Rodriguez Lozano, M.G. Velarde, Rev. Sci. Instrum. 63 (1992) 4208–4212.
[32] J.M.T. Thompson, H.B. Stewart, Nonlinear Dynamics and Chaos, Wiley, London, 1986.
[33] F. Schweitzer, W. Ebeling, B. Tilch, Phys. Rev. Lett. 80 (1998) 5044–5048.
[34] F. Schweitzer, Brownian Agents and Active Particles. Collective Dynamics in the Natural and Social Sciences, Springer, Berlin, 2003.
[35] W. Ebeling, I.M. Sokolov, Statistical Thermodynamics and Stochastic Theory of Nonequilibrium Systems, World Scientific, Singapore, 2005.
[36] B. Van der Pol, Phil. Mag. Ser. 2 (7) (1926) 978;
B. Van der Pol, Phil. Mag. Ser. 3 (7) (1927) 65.
[37] J.W. Strutt (Lord Rayleigh), Phil. Mag. 15 (1883) 229–232.
[38] J.W. Strutt (Lord Rayleigh), Theory of Sound, vol. I, Section 68, Dover reprint, New York, 1945.
[39] B. Tilch, F. Schweitzer, W. Ebeling, Physica A 273 (1999) 443–448.
[40] Y.-X. Li, X.-Z. Wu, Y.-Z. Zhuo, Physica A 286 (2000) 147–155.
[41] Y.-X. Li, Physica A 251 (1998) 382–388.
[42] M. Borromeo, F. Marchesoni, Phys. Lett. A 249 (1998) 199–203.
[43] W.T. Coffey, Yu.P. Kalmykov, J.T. Waldron, The Langevin Equation, World Scientific, Singapore, 2004.
[44] H. Risken, The Fokker-Planck Equation, Springer, Berlin, 1989 (Cap. 11).
[45] V. Heine, M.L. Cohen, D. Weaire, The Pseudopotential Concept, Academic Press, New York, 1970.